Scalar glueball mass reduction at finite temperature in SU(3) anisotropic lattice QCD

Noriyoshi Ishii
The Institute of Physical and Chemical Research (RIKEN), 2-1 Hirosawa, Wako, Saitama 351-0198, Japan

Hideo Suganuma
Tokyo Institute of Technology, 2-12-1 Ohkayama, Meguro, Tokyo 152-8552, Japan

Hideo Matsufuru
Yukawa Institute for Theoretical Physics, Kyoto University, Kitashirakawa-Oiwake, Sakyo, Kyoto 606-8502, Japan
(Received 17 August 2001; revised manuscript received 1 April 2002; published 30 July 2002)

We report the first study of the glueball properties at finite temperatures below T_c using SU(3) anisotropic lattice QCD with $\beta=6.25$, the renormalized anisotropy $\xi\equiv a_s/a_t=4$ and $20^3\times N_t(N_t=35,36,37,38,40,43,45,50,72)$ at the quenched level. From the temporal correlation analysis with the smearing method, about 20% mass reduction is observed for the lowest scalar glueball as $m_G(T)=1250\pm 50$ MeV for $0.8T_c<T<T_c$ in comparison with $m_G\simeq 1500$–1700 MeV at $T\simeq 0$.

DOI: 10.1103/PhysRevD.66.014507 PACS number(s): 12.38.Gc, 11.15.Ha, 12.38.Mh, 12.39.Mk

Finite temperature QCD, including quark gluon plasma (QGP) physics, is one of the most interesting subjects in quark hadron physics [1–3]. At high temperature, in accordance with the asymptotic freedom of QCD, the strong interaction among quarks and gluons is expected to be reduced, and deconfinement and/or a chiral phase transition would occur [1].

For the study of finite temperature QCD, lattice QCD Monte Carlo simulation provides a reliable method directly based on QCD. For instance, SU(3) lattice QCD simulations at the quenched level show a weak first-order deconfinement phase transition at the critical temperature $T_c\simeq 260$ MeV [4], and full SU(3) QCD simulations show a chiral phase transition at $T_c=173(8)$ MeV for $N_f=2$ and $154(8)$ MeV for $N_f=3$ in the chiral limit [5]. Above T_c, most of the nonperturbative properties such as color confinement and spontaneous chiral-symmetry breaking disappear, and quarks and gluons are liberated.

Even below T_c, there are many model predictions on the change of the hadron properties [2,6,7], the mass and the size, due to the change in the interquark potential [8,9] and the partial chiral restoration. As a precritical phenomenon of the QCD phase transition, the possible hadron mass shift at the finite temperature or in the finite density is now one of the most interesting subjects in hadron and QGP physics. For instance, the CERES data with the ultrarelativistic heavy-ion collision experiment may indicate the ρ-meson mass shift [10], and many theoretical studies [11] have been done to explain this experiment.

Nevertheless, lattice QCD studies for thermal properties of hadrons are still inadequate at present because of the difficulty in measuring the hadronic two-point correlators on the lattice at finite temperature. For instance, on the screening-mass measurement [12], this difficulty is due to the mixture of the large Matsubara frequencies in addition to the absence of technical prescriptions as the smearing method. On the other hand, on the pole-mass measurement, while it is free from the mixture of the Matsubara frequencies, another difficulty arises from the shrink of the physical temporal size $1/T$ at high temperature. In fact, the pole-mass measurements have to be performed within the limited distance shorter than $1/(2T)$, and such a limitation corresponds to $N_t=4$–8 near T_c in the ordinary isotropic lattice QCD [4].

To avoid this severe limitation on the temporal size, we adopt an anisotropic lattice where the temporal lattice spacing a_t is smaller than the spatial one a_s [8,13–15]. We can thus efficiently use a large number of the temporal lattice points as $N_t\sim 32$ even near T_c, while the physical temporal size is kept fixed $1/T=N_t a_t$. In this way, the number of available temporal data is largely increased, and accurate pole-mass measurements from the temporal correlation become possible [14,15].

In this paper we study the glueball at finite temperature from the temporal correlation analysis. We use SU(3) anisotropic lattice QCD at the quenched level, as a necessary first step before attempting to include the effects of dynamical quarks in the future. Even without dynamical quarks, quenched QCD can reproduce well various masses of hadrons, mesons, and baryons, and important nonperturbative quantities such as the confining force and the chiral condensate. In quenched QCD, unlike full QCD, the elementary excitations are only glueballs in the confinement phase below $T_c\simeq 260$ MeV. At zero temperature, the lightest physical excitation is a scalar glueball with $J^{PC}=0^{++}$ with the mass $m_G\simeq 1500$–1700 MeV [15–18], which is expected to dominate the thermodynamical properties below T_c.

We consider the glueball correlator [15–20] in SU(3) lattice QCD as $G(t)\equiv\langle\tilde{O}(t)\tilde{O}(0)\rangle$, $\tilde{O}(t)\equiv O(t)-\langle O\rangle$, $O(t)\equiv\Sigma_{\vec{x}}O(t,\vec{x})$. The summation over $\vec{x}$ physically means the zero-momentum projection. The glueball operator $O(t,\vec{x})$ is to be properly taken so as to reproduce its quantum number J^{PC} in the continuum limit. For instance, the simplest composition for the scalar glueball is given as $O(t,\vec{x})\equiv \mathrm{Re\,Tr}\{P_{12}(t,\vec{x})+P_{23}(t,\vec{x})+P_{31}(t,\vec{x})\}$, where

$P_{\mu\nu}(t,\vec{x}) \in$ SU(3) denotes the plaquette operator. With the spectral representation, $G(t)$ is expressed as $G(t)/G(0) = \Sigma c_n e^{-E_n t}$, $c_n \equiv |\langle n|\tilde{O}|0\rangle|^2/G(0)$, $G(0) = \Sigma|\langle n|\tilde{O}|0\rangle|^2$, where E_n denotes the energy of the nth excited state $|n\rangle$. Here, $|0\rangle$ denotes the vacuum, and $|1\rangle$ denotes the ground-state glueball. Note that c_n is a non-negative number with $\Sigma c_n = 1$. On a fine lattice with the spacing a, the simple plaquette operator $P_{ij}(t,\vec{x})$ has a small overlap with the glueball ground state $|G\rangle \equiv |1\rangle$, and the extracted mass looks heavier owing to the excited-state contamination. This small overlap problem originates from the fact that $O(t,\vec{x})$ has a smaller "size" of $O(a)$ than the physical peculiar size of the glueball. This problem becomes severer as $a \to 0$. We thus have to improve $O(t,\vec{x})$ so as to have almost the same size as the physical size of the glueball.

One of the systematic ways to achieve this is the smearing method [20–22]. The smearing method is expressed as the iterative replacement of the original spatial link variables $U_i(s)$ by the associated fat link variables, $\overline{U}_i(s) \in \mathrm{SU}(3)_c$, which is defined so as to maximize

$$\mathrm{Re\,Tr}\left[\overline{U}_i^{\dagger}(s)\left(\alpha U_i(s) + \sum_{j \neq i,\pm} U_{\pm j}(s) U_i(s \pm \hat{j}) U_{\pm j}^{\dagger}(s+\hat{i})\right)\right], \tag{1}$$

where $U_{-\mu}(s) \equiv U_{\mu}^{\dagger}(s-\hat{\mu})$, and α is a real parameter. Here, the summation is taken only over the spatial direction to avoid the nonlocal temporal extension. Note that $\overline{U}_i(s)$ holds the same gauge transformation properties with $U_i(s)$. We refer to the fat link defined in Eq. (1) as the first fat link $U_i^{(1)}(s)$. The nth fat link $U_i^{(n)}(s)$ is defined iteratively as $U_i^{(n)}(s) \equiv \overline{U}_i^{(n-1)}(s)$ staring from $U_i^{(1)} \equiv \overline{U}_i(s)$ [22]. For the physically extended glueball operator, we use the nth smeared operator, the plaquette operator constructed with $\overline{U}_i^{(n)}(s)$.

The smeared operator physically corresponds to an extended composite operator with the original field variable as $U_\mu(s)$. We consider the size of the nth smeared operator in terms of the original field variable. Using the linearization on the gluon field, we obtain the diffusion equation as [15,23]

$$\frac{\partial}{\partial n} K(\vec{x},n) = D \triangle K(\vec{x},n), \quad D \equiv \frac{a_s^2}{\alpha+4} \tag{2}$$

for the distribution $K(\vec{x},n)$ of the gluon field in the nth smeared plaquette, in the case of the small spatial lattice spacing a_s. The nth smeared plaquette located at the origin $\vec{x} = \vec{0}$ physically corresponds to the Gaussian extended operator with the distribution as [15,23]

TABLE I. The lattice QCD result for the lowest scalar glueball mass at finite temperature. The temporal lattice size N_t, the corresponding temperature T, the lowest scalar glueball mass $m_G(T)$, the maximal ground-state overlap $C^{\max}$, fully correlated χ^2/N_{DF}, the smearing number N_{smr}, the number of gauge configurations N_{conf} and the rough estimate of the glueball size ρ are listed. The most suitable smearing number N_{smr} is determined with the maximum ground-state overlap condition.

N_t	T(MeV)	m_G(MeV)	$C^{\max}$	χ^2/N_{DF}	N_{smr}	N_{conf}	ρ (fm)
72	130	1450(40)	0.93(2)	1.43	39	5541	0.42
50	187	1410(46)	0.92(3)	0.34	41	5168	0.44
45	208	1456(34)	0.96(1)	0.72	40	5929	0.43
43	218	1323(39)	0.89(2)	0.90	43	8693	0.45
40	234	1260(45)	0.84(3)	0.75	42	7420	0.44
38	246	1221(35)	0.85(2)	0.12	40	8736	0.43
37	253	1273(32)	0.88(2)	1.61	38	8633	0.42
36	260	1208(35)	0.84(2)	1.34	39	8603	0.42
35	268	1188(34)	0.84(2)	1.80	40	8462	0.43

$$K(\vec{x},n) = \frac{1}{(\pi\rho^2)^{3/2}} \exp\left[-\frac{\vec{x}^2}{\rho^2}\right], \tag{3}$$

where ρ represents the characteristic size of the Gaussian distribution, and is defined as

$$\rho \equiv 2\sqrt{Dn} = 2a_s\sqrt{\frac{n}{\alpha+4}}. \tag{4}$$

Thus, the smearing method, which is introduced to carry out the accurate mass measurement by maximizing the ground-state overlap, can be also used to give a rough estimate of the physical glueball size. In fact, once we obtain the maximum overlap with some n and α, the glueball size is roughly estimated with Eq. (4).

We use the SU(3) anisotropic lattice plaquette action

$$S_G = \frac{\beta}{N_c}\frac{1}{\gamma_{\mathrm{G}}} \sum_{s,i<j\leqslant 3} \mathrm{Re\,Tr}[1 - P_{ij}(s)] + \frac{\beta}{N_c}\gamma_{\mathrm{G}} \sum_{s,i\leqslant 3} \mathrm{Re\,Tr}[1 - P_{i4}(s)] \tag{5}$$

with the plaquette operator $P_{\mu\nu}(s) \in$ SU(3) in the (μ,ν) plane. The lattice parameter is fixed as $\beta \equiv 2N_c/g^2 = 6.25$, and the bare anisotropy parameter is taken as $\gamma_{\mathrm{G}} = 3.2552$ so as to reproduce the renormalized anisotropy $\xi \equiv a_s/a_t = 4$ [13]. These parameters produce the spatial lattice spacing as $a_s^{-1} = 2.341(16)$ GeV ($a_s \simeq 0.084$ fm), and the temporal one as $a_t^{-1} = 9.365(66)$ GeV ($a_t \simeq 0.021$ fm). Here, the scale unit is determined by adjusting the string tension as $\sqrt{\sigma} = 440$ MeV from the on-axis data of the static interquark potential. The pseudo-heat-bath algorithm is used to update the gauge field configurations on the lattice of the sizes 20^3

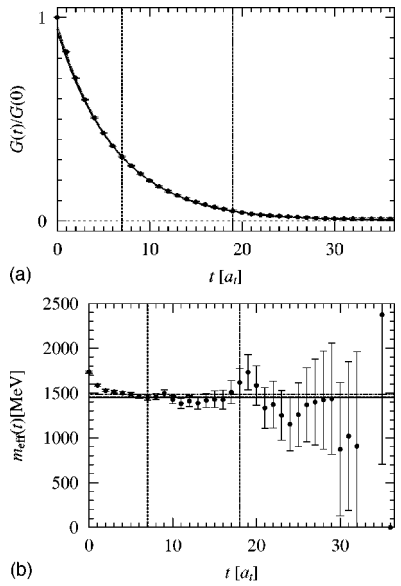

FIG. 1. (a) The scalar glueball correlator $G(t)/G(0)$ for $N_{\rm smr}=40$ at a low temperature $T=130$ MeV. (b) The corresponding effective mass plot. The statistical errors are estimated with the jackknife analysis. The solid line denotes the best single hyperbolic cosine fit to the lattice data in the interval $[t_{\rm min},t_{\rm max}]$ indicated by the two vertical dashed lines. The dashed and dotted curves are the best hyperbolic cosine curves for the modified fit range with $t_{\rm min}+1$ and $t_{\rm min}+2$, respectively. The closeness of the three curves means small fit-range dependence.

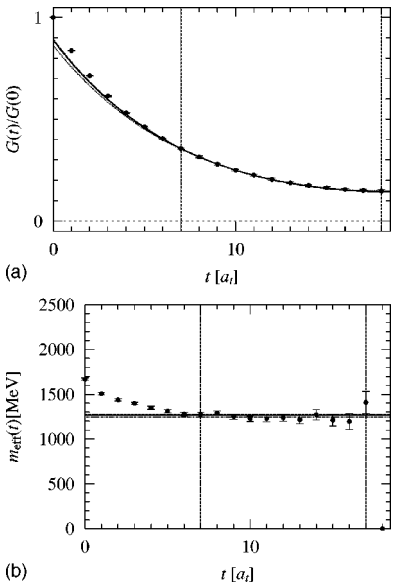

FIG. 2. (a) The scalar glueball correlator $G(t)/G(0)$ for $N_{\rm smr}=40$ at a high temperature $T=253$ MeV. (b) The corresponding effective mass plot. The statistical errors are estimated with the jackknife analysis. The solid line denotes the best single hyperbolic cosine fit to the lattice data in the interval $[t_{\rm min},t_{\rm max}]$ indicated by the two vertical dashed lines. The dashed and dotted curves are the best hyperbolic cosine curves for the modified fit range with $t_{\rm min}+1$ and $t_{\rm min}+2$, respectively. The closeness of the three curves means small fit-range dependence.

$\times N_t$, with $N_t=35,36,37,38,40,43,45,50,72$ as listed in Table I. For each temperature, we pick up gauge field configurations every 100 sweeps for measurements, after skipping more than 20,000 sweeps of the thermalization. The numbers of gauge configurations used in our calculations are summarized in Table I.

For completeness, we give an estimate of the critical temperature T_c. To this end, we analyze the scattering plot of the Polyakov loop $P(\vec{x})\equiv{\rm Tr}\{U_4(\vec{x},0)\cdots U_4(\vec{x},N_t-1)\}$ at each gauge field configuration. From this analysis, the $\mathbb{Z}_3$ symmetry holds at $N_t=35$, and the system is found to be in the confinement phase. On the other hand, the $\mathbb{Z}_3$ symmetry is broken at $N_t=34$, which indicates the deconfinement phase. Hence, we estimate $T_c\simeq 270$ MeV, which is consistent with the previous studies [4,8].

We present the numerical results in SU(3) anisotropic lattice QCD at the quenched level. To enhance the ground-state contribution, we adopt the smearing method with the smearing parameter $\alpha=2.1$, which we find one of the most suitable values from the numerical tests with various α. The statistical errors are estimated with the jackknife analysis [19].

In Fig. 1(a) we show a scalar glueball correlator $G(t)/G(0)$ at a low temperature $T=130$ MeV for the smearing number $N_{\rm smr}=40$, where most of the lattice QCD data are well fitted by a single hyperbolic cosine, denoted by the solid curve, as

$$G(t)/G(0)=C(e^{-m_G t a_t}+e^{-m_G(N_t-t)a_t}). \qquad (6)$$

This indicates the achievement of the ground-state enhancement owing to the smearing method, and then the excited-state contamination is almost removed.

In general, $G(t)/G(0)$ is expressed as a weighted sum of hyperbolic cosines with non-negative weights, and $G(t)/G(0)$ decreases more rapidly than Eq. (6) near $t=0$ due to excited-state contributions. Hence, C should satisfy the inequality $C\leqslant(1+e^{-m_G a_t N_t})^{-1}\simeq 1$. In the ground-state dominant case, $G(t)/G(0)$ can be well approximated by a single hyperbolic cosine, and $C\simeq 1$ is realized. We refer to C as the ground-state overlap.

From Fig. 1(a) we find $C\simeq 1$ and $m_G\simeq 1450$ MeV for the lowest scalar glueball mass at a low temperature. This seems consistent with $m_G\simeq 1500$–1700 MeV at $T\simeq 0$ [16–18].

In Fig. 2(a) we show a scalar glueball correlator $G(t)/G(0)$ at a high temperature $T=253$ MeV for the smearing number $N_{\rm smr}=40$. Owing to a suitable smearing, most of the lattice QCD data are well fitted by a single hyperbolic cosine denoted by the solid curve.

Each best fit analysis is performed in the interval $[t_{\rm min},t_{\rm max}]$, which is determined from the flat region $[t_{\rm min},t_{\rm max}-1]$ appeared in the corresponding ''effective mass'' plot shown in Figs. 1(b) and 2(b). The effective mass $m_{\rm eff}(t)$ is a solution of

$$\frac{G(t+1)}{G(t)}=\frac{\cosh[m_{\rm eff}(t)a_t(t+1-N_t/2)]}{\cosh[m_{\rm eff}(t)a_t(t-N_t/2)]}, \qquad (7)$$

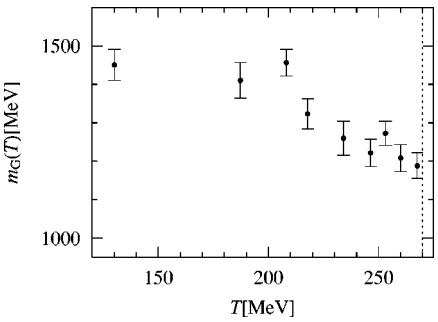

FIG. 3. The lowest scalar glueball mass plotted against the temperature T. It is obtained with the best hyperbolic cosine fit in the interval $[t_{\min},t_{\max}]$ determined from the flat region in the effective mass plot. The vertical dotted line indicates $T_c \simeq 270$ MeV.

for a given $G(t+1)/G(t)$ at each fixed t [19]. In Figs. 1 and 2, we show also the results of further two fits in the modified interval as $[t_{\min}+1,t_{\max}]$ and $[t_{\min}+2,t_{\max}]$ by dashed line and dotted line, respectively. The closeness of the three curves suggests small fit-range dependence.

In the most suitable smearing $N_{\rm smr}$, the ground-state overlap C is maximized and the mass m_G is minimized, which indicates the achievement of the ground-state enhancement. (For extremely large $N_{\rm smr}$, the operator size exceeds the physical glueball size, resulting in the decrease of the overlap C.) In practical calculations, the maximum overlap and the mass minimization are achieved at almost the same $N_{\rm smr}$, and both of these two conditions would work as an indication of the maximal ground-state enhancement. Here, we take the maximum ground-state overlap condition as $C \simeq 1$. (The mass minimization condition leads to almost the same glueball mass [23].)

From the analysis at various temperatures, we plot the lattice QCD result for the lowest scalar glueball mass $m_G(T)$ against temperature T in Fig. 3. We observe, in Fig. 3, about 20% mass reduction or a few hundred MeV mass reduction of the lowest scalar glueball near T_c as $m_G(T)=1250 \pm 50$ MeV for $0.8T_c<T<T_c$ in comparison with $m_G(T \sim 0) \simeq 1500$–$1700$ MeV [16–18].

We also give a rough estimate of the glueball size. To estimate the glueball size, we search $N_{\rm smr}$ which realizes the maximum ground-state overlap $C^{\max}$. From Eq. (4) with this $N_{\rm smr}$, we roughly estimate the glueball size as $\rho \simeq 0.4$–0.45 fm both at low temperature and at high temperature near T_c. Thus, we see that the thermal effect on the glueball size is rather small, which may provide important information in the bag model argument of the QCD phase transition [15,23].

In Table I we summarize the lowest scalar glueball mass $m_G(T)$, the ground-state overlap $C^{\max}$, fully correlated $\chi^2/N_{\rm DF}$, the corresponding smearing number $N_{\rm smr}$, the number of gauge configurations $N_{\rm conf}$, and the estimated glueball size ρ.

Thus, the present lattice QCD calculation indicates that the lowest scalar glueball exhibits about 250 MeV mass reduction near T_c keeping its size. Here, we briefly discuss the physical consequence of this result, considering the trigger of the QCD phase transition. In quenched QCD below T_c, the lowest glueball is the lightest particle, and its thermal excitation is expected to have primary relevance at finite temperature. However, lattice QCD indicates $m_G > 1$ GeV even near T_c, and therefore the thermodynamical contribution of the glueball seems strongly suppressed by the small statistical factor as $e^{-m_G/T}$ near $T_c \simeq 260$ MeV [15,23]. This may indicate that the thermal glueball excitation does not play the relevant role in the deconfinement phase transition, at least in quenched QCD. Then, what is the driving force to bring the phase transition? In this way, our result brings up such an interesting new puzzle on the QCD phase transition.

Several comments are in order. The first comment is on the closeness of our simulations to the continuum limit. In Ref. [24] the authors investigated β dependence of glueball masses at zero temperature, and estimated the discretization error on the scalar glueball mass to be less than 5% at $\beta=6.4$. According to them, the discretization error is estimated about 6% at $\beta=6.25$ in the present calculation. The second comment is on the finite volume artifact on the scalar glueball mass. In Ref. [16], Monte Carlo simulations were performed on the lattice of the physical size $(1.76 \text{ fm})^3$ and $(1.32 \text{ fm})^3$ at zero temperature to investigate the finite volume errors in the various glueball masses by using an improved action. The authors concluded that the systematic error in the lowest scalar glueball mass from the finite volume is negligible at zero temperature. Note that the finite volume artifact on the scalar glueball mass is essentially independent of the regularization method, i.e., a specific choice of the lattice action, as far as the discretization is enough fine. It follows that, the finite volume artifact of our results are negligible, since the physical size of our lattice is $(1.68 \text{ fm})^3$.

To summarize, we have studied the glueball properties at finite temperature using SU(3) anisotropic quenched lattice QCD with 5000–9000 gauge configurations at each temperature. From the temporal correlation analysis with the smearing method, we have observed about 20% mass reduction of the lowest scalar glueball as $m_G(T)=1250 \pm 50$ MeV for $0.8T_c<T<T_c$, while no significant change is seen for meson masses near T_c in lattice QCD [14].

Finally, we comment on the brief outlook. It seems interesting to investigate other glueballs such as the 2^{++} glueball at finite temperature to clarify whether the thermal mass reduction is peculiar to the lowest scalar glueball or universal feature in glueballs. It would be also interesting to analyze the spectral function of the glueball at finite temperature from its temporal correlation in terms of the mass and the thermal width, because the width broadening may provide the similar effect to the temporal correlator [11] as the mass reduction. Our result shows that the scalar glueball mass reduction is about 250 MeV, which is enough large, and therefore the thermal mass shift of the scalar glueball may become observable in future experiments at the BNL Relativistic Heavy Ion Collider (RHIC).

H.S. was supported by the Grant for Scientific Research (No. 12640274) from the Ministry of Education, Culture, Science and Technology, Japan. H.M. is supported by Japan Society for the Promotion of Science for Young Scientists. The lattice calculations have been performed on NEC-SX5 at Osaka University.

[1] W. Greiner and A. Schäfer, *Quantum Chromodynamics* (Springer-Verlag, Berlin, 1994), p. 1.
[2] T. Hashimoto, K. Hirose, T. Kanki, and O. Miyamura, Phys. Rev. Lett. **57**, 2123 (1986).
[3] T. Matsui and H. Satz, Phys. Lett. B **178**, 416 (1986).
[4] G. Boyd, J. Engels, F. Karsch, E. Laermann, C. Legeland, M. Lutgemeier, and B. Petersson, Nucl. Phys. **B469**, 419 (1996).
[5] F. Karsch, E. Laermann, and A. Peikert, Nucl. Phys. **B605**, 579 (2001).
[6] T. Hatsuda and T. Kunihiro, Phys. Rev. Lett. **55**, 158 (1985).
[7] H. Ichie, H. Suganuma, and H. Toki, Phys. Rev. D **52**, 2944 (1995).
[8] H. Matsufuru *et al.*, in *Proceedings of Quantum Chromodynamics and Color Confinement*, edited by H. Suganuma *et al.* (World Scientific, Singapore, 2001), p. 246.
[9] O. Kaczmarek, F. Karsch, E. Laermann, and M. Lutgemeier, Phys. Rev. D **62**, 034021 (2000).
[10] CERES Collaboration, G. Agakichiev *et al.*, Phys. Rev. Lett. **75**, 1272 (1995).
[11] V. L. Eletsky, B. L. Ioffe, and J. I. Kapusta, Eur. Phys. J. A **3**, 381 (1998); Nucl. Phys. **A661**, 514 (1999).
[12] C. DeTar and J. B. Kogut, Phys. Rev. Lett. **59**, 399 (1987); S. Datta and S. Gupta, Nucl. Phys. **B534**, 392 (1998).
[13] T. R. Klassen, Nucl. Phys. **B533**, 557 (1998).
[14] QCD-TARO Collaboration, P. de Forerand *et al.*, Phys. Rev. D **63**, 054501 (2001).
[15] N. Ishii, H. Suganuma, and H. Matsufuru, in *Proceedings of Lepton Scattering, Hadrons and QCD*, edited by A. W. Thomas *et al.* (World Scientific, Singapore, 2001), p. 252; in *Lattice 2001*, Proceedings of the XIXth International Symposium on Lattice Filed Theory, Berlin, Germany, edited by M. Müller-Preussker *et al.* [Nucl. Phys. B (Proc. Suppl.) **106-107**, 516 (2002)].
[16] C. J. Morningstar and M. Peardon, Phys. Rev. D **60**, 034509 (1999), and references therein.
[17] J. Sexton, A. Vaccarino, and D. Weingarten, Phys. Rev. Lett. **75**, 4563 (1995), and references therein.
[18] M. J. Teper, OUTP-98-88-P (1998), hep-th/9812187.
[19] I. Montvay and G. Münster, *Quantum Fields on a Lattice* (Cambridge University Press, Cambridge, England, 1994), p. 1.
[20] H. J. Rothe, *Lattice Gauge Theories* (World Scientific, Singapore, 1992), p. 1.
[21] APE Collaboration, Phys. Lett. B **192**, 163 (1987).
[22] T. T. Takahashi, H. Matsufuru, Y. Nemoto, and H. Suganuma, Phys. Rev. Lett. **86**, 18 (2001).
[23] N. Ishii, H. Suganuma, and H. Matsufuru (in preparation).
[24] UKQCD Collaboration, G. S. Balietaly, Phys. Lett. B **309**, 378 (1993).